GEOPHYSICS, VOL. 67, NO. 1 (JANUARY-FEBRUARY 2002); P. 271–281, 11 FIGS.
10.1190/1.1451799

Biot slow-wave effects in stratified rock

Steven R. Pride*, Eric Tromeur‡, and James G. Berryman**

ABSTRACT

The transmission of P-waves through the stratified layers of a sedimentary basin is modeled numerically using Biot theory. The effects on the transmissivity of frequency, angle of incidence, layer thickness, permeability and elastic compliance of the rocks are all considered. Consistent with previous analytical work, it is found that the equilibration of fluid pressure between the fine layers of a sedimentary sequence can produce significant P-wave attenuation at low frequencies. For this attenuation mechanism to act within the surface-seismic band (say, 3–300 Hz), we find that there must be layering present at the scale of centimeters to tens of centimeters. If the layering is restricted to layers of roughly 1 m thickness or greater, then for typical sandstone formations, the attenuation caused by the interlayer flow occurs below the seismic band of interest. Such low-frequency interlayer flow is called Biot slow-wave diffusion in the context of Biot theory and is likely to be the dominant source of low-frequency attenuation in a sedimentary basin, even for relatively tight and stiff reservoir rock; however, the effect is enhanced in more compliant materials. At higher frequencies, the generation of slow-waves at interfaces is also shown to significantly affect the P-wave scattering so long as the layers are sufficiently thin and sufficiently compliant. This effect on the P-wave scattering is shown to increase with increasing angle of incidence. Our work is limited to performing numerical experiments, with care given to making realistic estimates of all the material properties required. No attempt is made here to define an equivalent viscoelastic solid that allows for such slow-wave effects.

INTRODUCTION

Seismic waves propagating through fluid-saturated sediments or sedimentary rock induce a small amount of macroscopic fluid flow. Biot's (1956a, b, 1962) theory of mechanical wave propagation in porous materials is able to model such wave-induced relative flow. A P-wave propagating through a uniform sedimentary layer will create flow perpendicular to the wavefront from regions of compression toward regions of dilatation. The associated attenuation (as measured by an inverse quality factor Q^{-1}) is at a maximum at a relaxation frequency $\omega_{\rm vbl}$ corresponding to when viscous boundary layers (vbl) first begin to develop in the pores (i.e., when inertial forces of the fluid in each pore first become important relative to the viscous shear forces). The relative-flow model of Johnson et al. (1987) predicts that

$$\omega_{\rm vbl} = \frac{\eta}{\rho_f F k_o}, \tag{1}$$

where η is fluid viscosity, ρ_f is fluid density, F is the electrical formation factor, and k_o is the dc permeability. The permeability model of Thompson et al. (1987) shows that $Fk_o = \ell^2/226$, where ℓ is the breakthrough pore diameter in a mercury-invasion experiment. Thompson et al. (1987) measure ℓ, F, and k_o for 50 sandstones that span seven orders of magnitude of permeability to demonstrate the remarkable validity of their relation. Thompson's 50 sandstones have relaxation frequencies that lie in the range $10\,{\rm kHz} < \omega_{\rm vbl}/2\pi < 10^4\,{\rm kHz}$, with most being on the order of a few hundred kilohertz. In the surface-seismic band (frequencies less than a few hundred hertz) this attenuation, which is known as "Biot-global-flow" attenuation, is essentially negligible.

In the presence of heterogeneity at the porous continuum scale, additional attenuation mechanisms are possible that can lead to nonnegligible attenuation and dispersion in the surface-seismic band. In sedimentary basins, the dominant source of heterogeneity is the layering of the sediments. As first

Manuscript received by the Editor June 28, 2000; revised manuscript received February 16, 2001.
*Formerly Stanford University, Department of Geophysics, Mitchell Building, 397 Panama Mall, Stanford, California 94305; presently Université de Rennes 1, Campus Beaulieu, Bât. 15, 35042 Rennes Cedex, France. E-mail: spride@univ-rennes1.fr.
‡Université de Rennes 1, Campus Beaulieu, Bât. 15, 35042 Rennes Cedex, France.
**University of California, Lawrence Livermore National Laboratory, P.O. Box 808 L-200, Livermore, California 94551-9900. E-mail: berryman1@llnl.gov.

understood and modeled by White et al. (1975), a P-wave with wavelengths longer than the layer thicknesses will compress (or expand) many layers simultaneously. Since each layer has, in general, different compressional properties, the fluid-pressure changes in adjacent layers will be different, and the pressure will try to equilibrate by fluid-pressure diffusion (i.e., by viscous flow). Within the context of Biot's theory, the process of fluid-pressure diffusion is known as the "Biot slow-wave." The creation of slow-waves at an isolated interface through mode conversion from an incident P-wave was first observed experimentally by Plona (1980) [also see Chin et al. (1985) for a successful comparison between theory and experiment].

Thus, when wavelengths are larger than layer thicknesses, one may say that Biot slow-waves are always generated in order to equilibrate the fluid pressure between the layers. The fluid flow associated with this equilibration can lead to significant attenuation and dispersion in the seismic band. Such slow-wave-induced attenuation is at a maximum at a relaxation frequency ω_{sw} corresponding to when the fluid-pressure-diffusion skin depth (penetration length) is on the order of the layer spacing and that thus goes as

$$\omega_{sw} \approx \frac{K_f k_o}{\eta \phi h^2}, \tag{2}$$

where K_f is the fluid incompressibility, ϕ is a characteristic porosity of the layering (e.g., the average porosity), k_o is a characteristic permeability, and h is a characteristic layer thickness. For layer thicknesses on the order of a few centimeters or more and for permeabilities on the order of 100 md or less, equation (2) shows that the slow-wave effects are at a maximum for frequencies of a few tens of hertz or less; that is, at least for sufficiently thin layering (1–10 cm), such slow-wave effects will tend to be at a maximum in the surface-seismic frequency band. Larger layer thicknesses will reduce $\omega_{sw}/2\pi$ to frequencies below 1 Hz. Equation (2) is formally based on fluid-pressure diffusion through a stiff framework of grains; however, in the opposite limit of an infinitely compliant frame, we show below that ω_{sw} will only be reduced by a few percent.

The central question we explore in this paper is whether such Biot slow-wave effects are of sufficient importance that exploration seismologists should consider them when attempting to invert surface seismic or vertical seismic profile (VSP) data. The goal is not to define effective material properties, but simply to determine the combination of material properties in a sedimentary sequence that results in significant slow-wave effects.

Much work has already been performed on this problem and all the above comments have been understood (although perhaps not appreciated by the seismic community at large) since the initial work of White et al. (1975). In particular, White et al. model the low-frequency fluid-pressure equilibration between alternating layers of gas and liquid saturated sediments, while neglecting all scattering effects. Those authors obtain an explicit expression for the attenuation and dispersion of the P-wave caused by such interlayer fluid flow. Norris (1993) gives an asymptotic treatment of the same problem that allows him to decouple the fluid-pressure-diffusion (or slow-wave) process from the compressional-wave propagation. The analysis requires that the P-wave wavelengths are much greater than the characteristic length over which the porous-continuum material properties vary (and over which the effective material properties are determined). Within this low-frequency asymptotic limit, Norris determines the exact leading order contribution to the compressional wave's attenuation and dispersion caused by the fluid-pressure equilibration between alternating (periodic) layers. He reproduces the same attenuation and dispersion results of White et al. (1975), thus giving justification to the more heuristic approximations initially made by White et al.

Gurevich and Lopatnikov (1995) extend the analysis to allow for P-wave propagation in randomly layered sediments. Their analytical results for the attenuation and dispersion caused by interlayer flow (Biot slow waves) are obtained under the combined requirements that (1) variations of material properties between the various layers are small (a type of single-scattering approximation known as the "Bourret approximation" in the context of waves in random media) and (2) frequencies are sufficiently small that all P-wave scattering effects from the individual layers are negligible. To obtain analytical results, their approach requires assumptions to be made about the correlation function associated with the random layering. When they apply their theory to the special case of alternating layers, results very similar to those of Norris (1993) and White et al. (1975) are obtained (Norris and White et al. place no restrictions on the material contrasts, but their analytical results are limited to alternating layers).

Finally, Gelinsky and Shapiro (1997) and Gelinsky et al. (1998) extend the analysis of P-waves in randomly layered sediments to higher frequencies so that P-wave scattering from the layer interfaces is treated in addition to the slow-wave interlayer flow. The central approximation of this work is again that contrasts in material properties must be sufficiently small that single-scattering truncations are valid. They also obtain analytic results once an integrable correlation function is chosen for the random layering. Gelinsky et al. (1998) and Shapiro and Müller (1999) demonstrate that their analytical results are consistent with numerical results obtained using the so-called OASES software (see references in their article) that models waves in stratified media. All of the analytical results referenced above are limited to normal incidence (purely 1-D) plane-wave propagation.

The work discussed above has properly defined the physics that controls the fluid-pressure equilibration between adjacent layers and, most importantly, has provided analytical expressions for the effective low-frequency attenuation and phase velocity. Nonetheless, we feel that a systematic exploration of the importance of such effects for a variety of realistic sedimentary-layer sequences is lacking and that such a study could aid practical seismologists interested in whether such effects should be included in their forward modeling.

For these reasons, we have developed for this paper a numerical model of seismic waves in stratified porous materials based on Kennett's (1983) reflectivity approach that places no restrictions on either the material-property contrasts, the frequency, or the angle of incidence. We use the model to study the way that the amplitude and phase of transmitted P-waves are affected by the combined effects of Biot slow-wave generation, P-wave scattering, and intrinsic global-flow attenuation in various sedimentary sequences that we feel are reasonable representations of real-world conditions. In order to aid in the separation of slow-wave effects from P-wave scattering effects, we always run two numerical models: one that uses the full set of Biot equations, and another that retains the global-flow

attenuation and dispersion of the Biot theory but that completely neglects the generation and diffusion of slow waves.

To outline the paper, first we present the physical model in the next section. Then, some details of the numerical model are presented (the full algorithm is given in the Appendix), followed by a section enumerating our examples and the results obtained using the layer code. We summarize our main conclusions in the final section.

THE PHYSICAL MODEL

The governing equations for this study are those controlling wave propagation in uniformly saturated isotropic porous materials (Biot, 1962) with an assumed $e^{-i\omega t}$ time dependence:

$$\nabla \cdot \boldsymbol{\tau} = -\omega^2(\rho \mathbf{u} + \rho_f \mathbf{w}) \tag{3}$$

$$-\nabla p = -\omega^2 \rho_f \mathbf{u} - i\omega \frac{\eta}{k(\omega)} \mathbf{w} \tag{4}$$

$$\boldsymbol{\tau} = [(H - 4G/3)\nabla \cdot \mathbf{u} + C\nabla \cdot \mathbf{w}]\mathbf{I} + G\left[\nabla \mathbf{u} + (\nabla \mathbf{u})^T - \frac{2}{3}\nabla \cdot \mathbf{u}\,\mathbf{I}\right] \tag{5}$$

$$-p = C\nabla \cdot \mathbf{u} + M\nabla \cdot \mathbf{w}. \tag{6}$$

Here, $\boldsymbol{\tau}$ is the total average stress tensor acting on each sample of sedimentary rock, p is the average fluid pressure, $\mathbf{u}$ is the average displacement of solid grains, and $\mathbf{w}$ is the average relative fluid-solid displacement defined so that $-i\omega\mathbf{w}$ corresponds to the Fourier transform of the Darcy filtration velocity. The bulk density ρ of the rock is $\rho = (1-\phi)\rho_s + \phi\rho_f$, where ϕ is the porosity, ρ_f is the density of the pore fluid (always taken to be water in this study, so that $\rho_f = 10^3$ kg/m^3), and ρ_s is the average density of the grains in the rock (always taken as quartz, so that $\rho_s = 2.7 \times 10^3$ kg/m^3).

Biot's (1962) three incompressibility moduli ($H - 4G/3$, C, and M) can be expressed in terms of the three moduli that have the clearest laboratory definitions; namely, (1) the undrained bulk modulus K_U controlling the volumetric changes of a sealed sample, (2) the drained bulk modulus K_D controlling the volumetric changes of a sample under conditions where the fluid pressure does not change (sometimes called the "frame" modulus), and (3) Skempton's (1954) coefficient B, which is the ratio between the fluid-pressure and applied-confining-pressure increments for a sealed sample. These generally valid relations are

$$H - 4G/3 = K_U \tag{7}$$

$$C = BK_U \tag{8}$$

$$M = \frac{B^2}{1 - K_D/K_U} K_U, \tag{9}$$

being independent of the possible presence of anisotropy at either the sample or grain scale and of whether the grains making up the rock have different mineralogies. The modulus G is the shear modulus of a sample and will be taken here as being independent of the fluid properties. Note that upon taking the divergence of equation (4) and inserting equation (6), the fluid-pressure diffusion equation is obtained ($D_p \nabla^2 p + i\omega p =$ source terms), where

$$D_p = Mk/\eta \tag{10}$$

is the fluid-pressure diffusivity and defines the physical role played by M in the context of this study.

We next impose the restriction that the grains in each rock sample are both isotropic and homogeneous. Under such monomineral restrictions (and only under such conditions), the relations of Biot and Willis (1957) are valid. These relations give the explicit dependence of the porous-material moduli on the pore-fluid and solid-grain bulk moduli K_f and K_s, and can be written

$$B = \frac{1/K_D - 1/K_s}{1/K_D - 1/K_s + \phi(1/K_f - 1/K_s)}, \tag{11}$$

$$K_U = \frac{K_D}{1 - B(1 - K_D/K_s)}. \tag{12}$$

After some algebra, the following forms for the moduli prove to be instructive:

$$K_U = \frac{K_D + [1 - (1+\phi)K_D/K_s]K_f/\phi}{1 + \Delta}, \tag{13}$$

$$C = \frac{(1 - K_D/K_s)K_f/\phi}{1 + \Delta}, \tag{14}$$

$$M = \frac{K_f/\phi}{1 + \Delta}, \tag{15}$$

where Δ is a dimensionless parameter defined as

$$\Delta = \frac{1-\phi}{\phi}\frac{K_f}{K_s}\left(1 - \frac{K_D}{(1-\phi)K_s}\right). \tag{16}$$

The usefulness of writing the poroelastic moduli this way is that Δ is always a very small number. In an extreme stiff-frame limit defined by $K_D \to (1-\phi)K_s$ [which actually lies above the Hashin-Shtrikman (1961) upper bound], we have that $\Delta \to 0$. The opposite limit of an infinitely compliant frame $K_D \to 0$ occurs when the grains no longer form connected paths across the sample. In sediments, this percolation threshhold occurs when $\phi \approx 0.5$, with the precise value depending on details of the grain-size distribution and packing configuration. We thus have that Δ takes its largest value of K_f/K_s when there is an infinitely compliant frame and that Δ is never outside the range $0 < \Delta < K_f/K_s$ for any material type. This means in particular that the modulus M is bounded as $1/(1 + K_f/K_s) < \phi M/K_f < 1$. Since $K_f/K_s \approx 10^{-1}$ when the fluid is a liquid [all examples in this paper are calculated with $K_s = 36$ GPa (quartz) and $K_f = 2.2$ GPa (water)], the pressure diffusivity of equation (10) is always well approximated as $D_p \approx K_f k_o/(\eta\phi)$, which is the estimate used to obtain equation (2). However, we will make no such approximations in the numerical modeling that follows.

The drained modulus is a strong function of the microgeometery of the sample, and no universal law exists that relates it to, say, porosity. Nonetheless, in lower-porosity materials, the drained modulus is larger than in higher-porosity materials, and we propose that the simple rules

$$K_D = K_s \frac{1-\phi}{1 + a\phi}, \tag{17}$$

$$G = G_s \frac{1-\phi}{1 + b\phi} \tag{18}$$

are adequate for our purposes with a and b varying with lithology. Here, G_s is the shear modulus of the grain material ($G_s =$ 44 GPa for quartz). Effective medium theories (e.g., Korringa

et al., 1979; Berryman, 1980a, b) yield expressions of this form and predict that a and b depend on the shape of the assumed pores and on the ratio K_s/G_s; we assume here that K_s/G_s is a constant for all rocks and, indeed, it is close to one for most sand grains of interest. Depending on the degree of consolidation (i.e., the degree to which compliant, high-aspect-ratio porespace is present in and around the grain contacts), one can expect the approximate range $2 < a, b < 20$ for sandstones (2 being well consolidated and 20 poorly consolidated). However, an unconsolidated sand in this model can require $a \gg 20$. With these assumptions, the free parameters that fix the elastic properties are ϕ, a, and b. To remove a free parameter, we will somewhat arbitrarily take $b = 3a/2$ in all of our modeling (effective-medium theories predict $b > a$, and a factor of 3/2 is reasonable for consolidated sediments).

The last material property of the model is the dynamic permeability $k(\omega)$. Here, we use the previously mentioned result of Johnson et al. (1987):

$$\frac{k(\omega)}{k_o} = \left[\sqrt{1 - i\frac{\omega}{\omega_{\text{vbl}}}\frac{4}{n}} - i\frac{\omega}{\omega_{\text{vbl}}}\right]^{-1}, \tag{19}$$

where k_o is the dc permeability of the material, ω_{vbl} is the viscous-boundary-layer transition frequency defined in equation (1), and n is a dimensionless number that depends only on pore-geometery terms

$$n = \frac{\Lambda^2}{Fk_o}. \tag{20}$$

Here, F is again the electrical formation factor, while Λ is a weighted pore-volume to grain-surface-area ratio with the weight emphasizing constricted parts of the connected pore space. There is anectodal evidence suggesting that $n \approx 8$ for relatively clean sandstones and sediments. However, in rock with significant secondary clay growth, n is likely to decrease below this value; in other words, it is likely that n should not, in general, be considered a universal constant. Nonetheless, in order to reduce the number of free parameters, we will simply take $n = 8$ for all sediments modeled in this study. Finally, the dc permeability will be determined using the model of Thompson et al. (1987):

$$k_o = \frac{\ell^2}{226F}, \tag{21}$$

with Archie's law ($F = \phi^{-m}$) being used for the formation factor. The Archie exponent typically lies in the range $1.5 < m < 2.2$ for sedimentary rock, with variations due to differences in the microgeometery of rock. In order to eliminate yet another free parameter, we take $m = 1.7$ for all our sediments. Thompson et al. (1987) measured ℓ for their 50 sandstones and, with the exception of a single impermeable sample (having a permeability less than their experimental limit of roughly 1 μd), all the ℓ values lie in the range $0.3\ \mu\text{m} < \ell < 90\ \mu\text{m}$, with the variation depending on both the degree of secondary clay growth and the initial detrital grain sizes. This range in ℓ combined with the simultaneous variations in F corresponds to more than seven orders of magnitude in permeability variation.

Thus, in this work, a sedimentary sequence is defined by fixing the three physical properties of ϕ (porosity), a (the frame-compliance factor), and ℓ (the mercury-breakthrough pore diameter) for each layer of the sequence. In the examples section, we discuss our strategy for selecting these three numbers.

THE NUMERICAL MODEL

Our sedimentary sequence consists of a stack of L porous layers sandwiched between two porous half-spaces and having a total thickness $H = \sum_{\ell=1}^{L} h_\ell$, where the h_ℓ are the layer thicknesses. The naming convention for the layers and interfaces is shown in Figure 1. In general, there are downward-incident plane waves of any type [fast compressional waves (P), slow waves (slow), or vertically polarized shear waves (SV)] at the top of the stack, and we are interested in how these waves reflect from and transmit through the stack. If the downward-incident wave amplitudes are placed in a first-order array $\mathrm{d} = [\mathrm{d_P}, \mathrm{d_{slow}}, \mathrm{d_{SV}}]^T$ (these incident amplitudes can all be taken as unity), we determine here the complex reflected-wave "amplitudes" $r = [r_{\text{P}}, r_{\text{slow}}, r_{\text{SV}}]^T$ at the top of the stack and the transmitted-wave amplitudes $t = [t_{\text{P}}, t_{\text{slow}}, t_{\text{SV}}]^T$ that emerge at the bottom of the stack. Such linear response can be written

$$r = \mathcal{R}_0\,\mathrm{d} \quad \text{and} \quad t = \mathcal{T}_0\,\mathrm{d}, \tag{22}$$

where $\mathcal{R}_0$ and $\mathcal{T}_0$ are called the "total-reflection" and "total-transmission" matrices. In this paper, we use Kennett's reflectivity method (Kennett and Kerry, 1979) to calculate $\mathcal{R}_0$ and $\mathcal{T}_0$. The algorithm and all the required formulas are given in Appendix A.

For a unit-amplitude downward P-wave incident at the top of the stack $\mathrm{d} = [1, 0, 0]^T$, we focus specifically on the complex transmission through the stack $t_{\text{P}}(\omega, p)$ where p is the purely real horizontal slowness (ray parameter) that is constant in all layers. Expressing t_{P} in terms of amplitude and phase,

$$t_{\text{P}}(\omega, p) = e^{-\omega q_I(\omega,p)H} e^{i\omega q_R(\omega,p)H}, \tag{23}$$

then defines the effective complex vertical slowness $q_R(\omega, p) + iq_I(\omega, p)$ for the entire stack of thickness H, where q_R and q_I are both real. Because there is a finite delay for the response at $z = H$ to be recorded when a temporal point source acts at $z = 0$, it is a standard excercise (e.g., Aki and Richards, 1980) to show that $t_{\text{P}}(\omega)$ is free of both singularities and zeros in the upper half ω plane. This fact then guarantees that

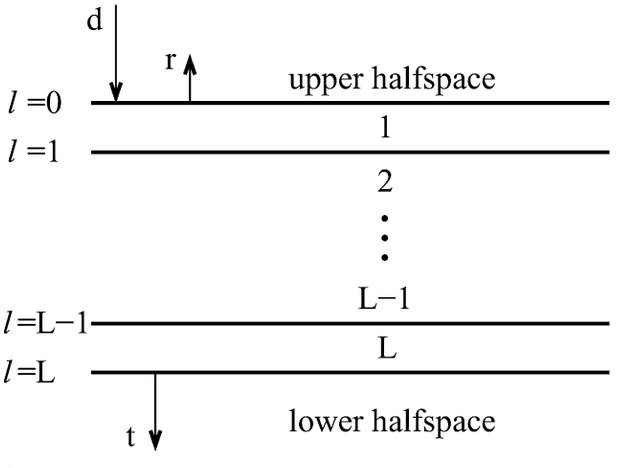

FIG. 1. The naming convention of the interfaces and layers of the sedimentary sequence.

$\ln t_P = -\omega q_I(\omega)H + i\omega q_R(\omega)H$ is also free of singularities in the upper half ω plane, and such analyticity in turn guarantees that $q_R(\omega)$ and $q_I(\omega)$ are Hilbert transforms of each other. All of this holds independently of what happens to the P-wave in the stack, so long as what happens there both respects the laws of physics and remains linear with respect to the incident-wave amplitudes.

Following the authors cited in the Introduction, we elect to present q_R and q_I as a function of frequency and in the following representation:

$$v = 1/q_R \quad \text{and} \quad Q^{-1} = 2q_I/q_R, \tag{24}$$

where Q is an effective quality factor for the stack, and v is an effective vertical phase velocity. However, we emphasize that the stack properties v and Q^{-1}, so determined, are in no way intended to define effective-medium properties for use in seismic forward modeling. Effective-medium properties in wave problems are meaningfully defined only when the heterogeneity over which one averages to obtain them is smaller than the pulse length of the wave. The goal of this study is to quantify the extent to which slow waves can affect the P-wave transmission process regardless of the relation between heterogeneity size and wavelength. The stack properties v and Q^{-1} are simply a familiar way to represent the filter t_P.

In order to quantify the role of the slow wave, we also calculate the response determined using the usual elastodynamic equations for a nonporous solid. The eigenvectors of an elastic solid (that are required in the reflectivity scheme) are easily determined and can be found, for example, in Aki and Richards (1980). For these calculations, we use the complex phase slownesses s_P and s_{SV} of the Biot theory (see Appendix A) and call the results so determined the "viscoelastic" response. Such response includes all P-SV scattering and Biot global-flow intrinsic attenuation, but neglects entirely the generation and diffusion of Biot slow-waves.

In what follows, the properties of the two semi-infinite bounding spaces are taken to be identical and are required to have the following average properties of the stack: $K_D^{hs} = 1/\langle K_D^{-1}\rangle$, $G^{hs} = 1/\langle G^{-1}\rangle$, $k_o^{hs} = 1/\langle k_o^{-1}\rangle$, and $\phi = \langle\phi\rangle$, where the brackets denote depth averaging over the stack.

EXAMPLES

We now carry out the above scheme. To do so requires that the numbers ϕ, a, and ℓ have been selected for each layer of a studied sequence. We determine these numbers and thus develop lithological sequences in two different ways.

The Blackhawk-sandstone formation

First, the sandstone data of Thompson et al. (1987) is used. These authors measure ϕ, ℓ, and P-wave velocity on their cores, and we select the frame-compliance factor a of equation (17) so as to match their measured P-wave velocity. In particular, Thompson et al. studied a set of 36 cores all taken from the same well in the Blackhawk sandstone formation in Utah. We took the measured properties of these 36 cores and made a lithological sequence of 72 layers having random thicknesses. The cores were taken from several different depth sections and, in our layer model, we preserve the relative positioning of cores coming from the same depth section. The layer thicknesses were calculated using

$$h = yh_{\min} + (1-y)h_{\max}, \tag{25}$$

where y is a random number that varies uniformly between 0 and 1, with $h_{\min}$ and $h_{\max}$ thus constraining the thinnest and thickest layers in the sequence.

Figure 2 shows three key material properties as a function of depth when $h_{\min} = 10$ cm and $h_{\max} = 1$ m. Figure 3 shows the associated transmission response (v, Q^{-1}); also shown is the relative difference between the viscoelastic Q_v^{-1} and poroelastic Q_p^{-1} attenuation. Three primary frequency regimes are observed: (1) a low-frequency regime (<10 Hz) in which the attenuation is controlled by the slow-wave diffusion; (2) a middle-frequency regime (10–10^5 Hz) in which P-wave scattering is the principal loss mechanism; and, finally, (3) a high-frequency regime (>10^5 Hz) in which viscous boundary layers finally begin to develop in the pores with an associated peak (at roughly 3 MHz) in the global-flow viscous attenuation. The difference between the poroelastic and viscoelastic results is entirely due to the generation of slow waves. In this example, the generation of slow waves is seen to have no noticeable effect on the P-wave scattering process. The P-wavelengths became smaller than all layer thicknesses at a frequency of about 35 kHz. After careful testing, we believe that the small spikes in the difference of attenuation plots ($1 - Q_p/Q_v$) are true slow-wave effects and not just numerical artifacts. In a later example, it will be seen that slow-wave effects can be very important in the P-wave scattering regime if the layer spacing is thin enough and if the material is both compliant and permeable.

In this and all the following examples, the onset of the scattering regime is characterized by a first band of attenuation variation (between 5 and 50 Hz in Figure 3) that consistently has a peak when the average P-wavelength is roughly four

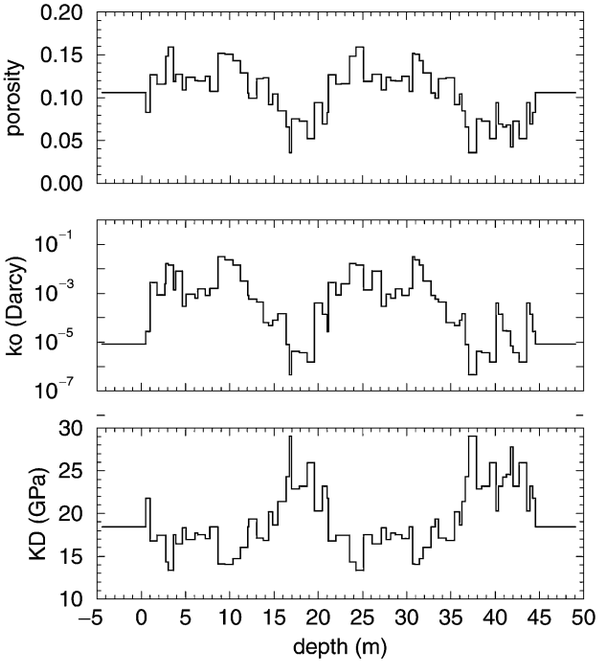

FIG. 2. Our representation of the porosity, permeability, and drained bulk modulus of the Blackhawk sandstone formation in Utah. The properties of each of the 72 layers are derived from the laboratory measurements of Thompson et al. (1987).

times the total stack thickness H (about 20 Hz in Figure 3). As stated, we have chosen the half-spaces to contain the average elastostatic properties of the stack. If the half-spaces are allowed to have arbitrary properties, this attenuation due to the destructive interference at the scale of H is significantly enhanced.

From a surface-seismic perspective, the slow waves are not playing an important role in this example. Because the Blackhawk formation has a rather low average permeability, the regime of interlayer flow occurs at frequencies below the surface-seismic band. Equation (2) indicates when such interlayer flow is important.

In a second example (Figure 4), we preserve everything about the Blackhawk sequence of Figure 2 except that the individual layer thicknesses are allowed to range between 60 cm and 6 m (six times greater than in Figure 2). As expected, the main effect of increasing the layer thickness is to shift the band where interlayer flow occurs to still lower frequencies. The magnitudes of both the interlayer-flow attenuation and scattering losses are essentially unchanged relative to the previous example; only the frequency at which these mechanisms occur has been significantly altered.

The more important case of having thinner layers will be considered in the next section.

Synthetic sequences

In order to study the effects of altering material properties other than layer thickness, we produce a series of purely synthetic lithological sequences. Our approach here is to fix a benchmark sequence and then make changes relative to the benchmark. In these examples, we investigate the sensitivity of the transmissivity to permeability, frame compliance, and angle of incidence. We conclude with an example having fine layering and an interesting constant Q behavior in the seismic band.

To generate the values of ϕ, a, and ℓ in our synthetic sequences, we note that these numbers are not entirely independent since they all will tend to change depending on the degree of secondary mineral growth. If x is a random number uniformly lying between 0 and 1 and representing the "shalyness" of a rock layer (with 0 repesenting the least secondary growth and least consolidation), we build a sequence of random layers using a random number generator for x and the following rules:

$$\phi = x\phi_{\min} + (1-x)\phi_{\max}, \tag{26}$$

$$a = x^{1+\epsilon_a} a_{\min} + (1 - x^{1+\epsilon_a}) a_{\max}, \tag{27}$$

$$\ell = x^{1-\epsilon_\ell} \ell_{\min} + (1 - x^{1-\epsilon_\ell}) \ell_{\max}. \tag{28}$$

These rules were chosen for their simplicity. Note that because our interest here is with layering at scales finer than the 1-m resolution usually provided by well logs, we don't feel justified in using statistics derived from well logs. Exponents on x that are greater than one tend to favor the upper end of a given range, whereas exponents less than one favor the lower end (ϵ_a and ϵ_ℓ are both positive). Thus we use $x^{1-\epsilon_\ell}$ for the breakthrough pore diameter ℓ so as to favor lower permeabilities and $x^{1+\epsilon_a}$ for the consolidation factor a in order to favor weaker frame moduli, the logic being that secondary clay has a relatively larger effect in bringing down permeability

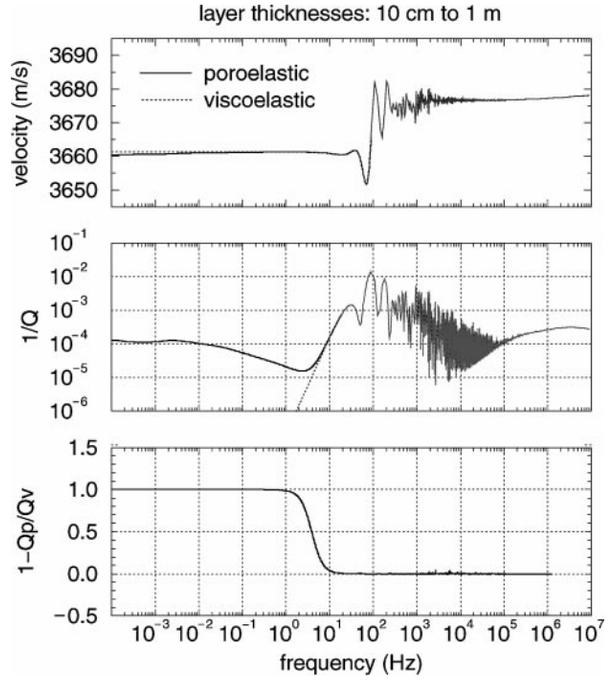

FIG. 3. Phase velocity, Q^{-1}, and the relative difference $(Q_p^{-1} - Q_v^{-1})/Q_p^{-1}$ (p = poroelastic and v = viscoelastic) for the Blackhawk formation as presented in Figure 2. The observed difference between the poroelastic attenuation and the viscoelastic attenuation is entirely due to slow waves in this model.

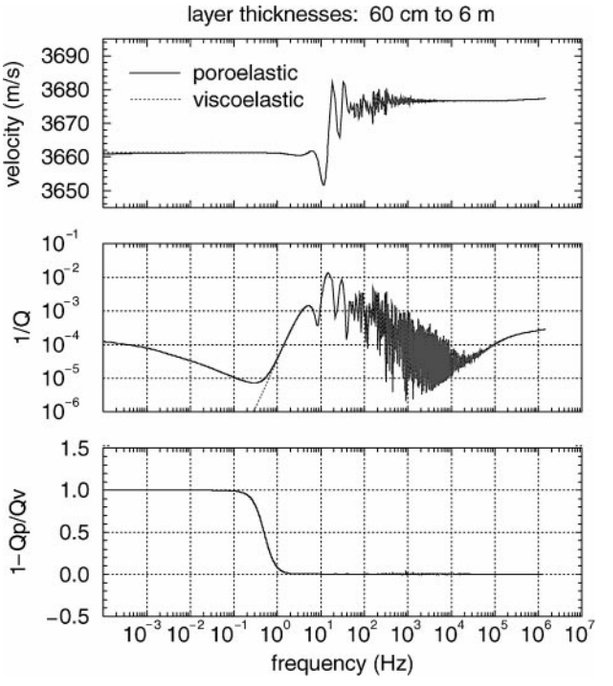

FIG. 4. The same Blackhawk formation as in Figure 2, except layer thicknesses range from 60 cm to 6 m instead of 10 cm to 100 cm. The low-frequency interlayer-flow attenuation has now been shifted to frequencies well below the seismic band of interest.

than in strengthening the framework of grains. Different lithological sequences can be made by altering the minimum and maximum values of ϕ, a, and ℓ for the sequence and/or by altering the exponents ϵ_a and ϵ_ℓ of the shalyness coefficient x. In all the following examples, we somewhat arbitrarily take $\epsilon_a = \epsilon_\ell = 1/3$. Layer thicknesses h are again taken from equation (25) with y being a different random number than x.

This model produces a sequence in which the material properties change in a physically consistent manner; however, there are endless possible generalizations, some of which might include: allowing for the effects of secondary quartz as distinct from secondary clay (for the same effect on porosity, secondary quartz can dramatically increase the rock strength as compared to secondary clay); allowing explicitly for separate pure shale layers; choosing the shalyness coefficients (or other properties) from a more complicated probability density function; building in trends with depth (e.g., overburden-induced effective-pressure dependence of the material properties); allowing for fluid overpressure zones; allowing for various mixes of gas/oil/water; allowing for fractal layer thicknesses; etc. Nonetheless, our simple model is sufficient for our limited purposes here.

The benchmark sequence.—We first establish the benchmark sequence by defining the following range of our three lithological parameters: $0.05 < \phi < 0.25, 2\ \mu\text{m} < \ell < 20\ \mu\text{m}, 3 < a < 6$. This sequence is just slightly more compliant and significantly more permeable than the Blackhawk sequence. The key physical properties of this benchmark sequence are shown in Figure 5, and the associated v and Q^{-1} are shown in Figure 6. Normally incident waves have again been used, and the layer thicknesses again lie between 10 cm and 1 m. For this benchmark sequence, interlayer-flow attenuation begins to be important in the lower end of the surface-seismic band.

We have only taken 30 layers for this and all the following examples so that run times are kept reasonable. Note that in order to determine $q_R(\omega)$ [and, therefore, the vertical phase velocity $v(\omega)$] from the transmissivity given in equation (23), one must vary frequency on essentially a linear scale once wavelengths drop below the stack thickness H so that every cycle of 2π in the transmission's phase variation is accounted for. Our displayed plots typically require a few hundred thousand separate frequency evaluations, and it is therefore desirable to keep the run time low for each evaluated frequency. In addition, nothing particularly new about the questions we are addressing here is learned by increasing the number of layers.

Larger permeabilities.—This example investigates the effect of increasing the permeability of the benchmark sequence. To do so, we now let ℓ lie in the range $8\ \mu\text{m} < \ell < 80\ \mu\text{m}$, which corresponds roughly to increasing the permeabilities by a factor of 16. In Figure 7, we see that the peak in interlayer-flow attenuation has indeed been shifted by roughly a factor of 16 [as equation (2) predicts]. The result is merely a shift in center frequency; the magnitude of the interlayer-flow attenuation has not been altered by increasing the permeability. At higher frequencies, the slow-wave effects on the P-wave scattering are a bit more pronounced because the amplitude of a slow wave generated at an isolated interface increases with permeability.

Larger frame compliances.—This example investigates the effect of increasing the compliance of the framework of grains.

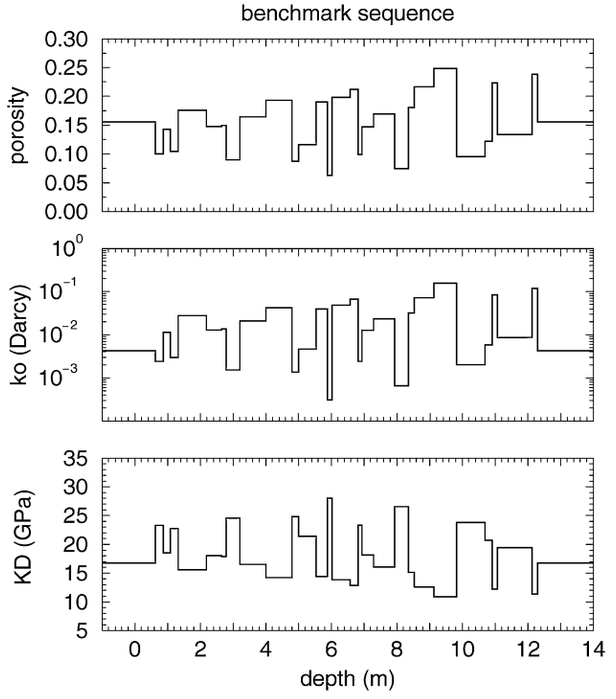

FIG. 5. The porosity, permeability, and drained bulk modulus of the "benchmark" synthetic sequence against which the following two examples (see Figures 6 and 7) will be compared.

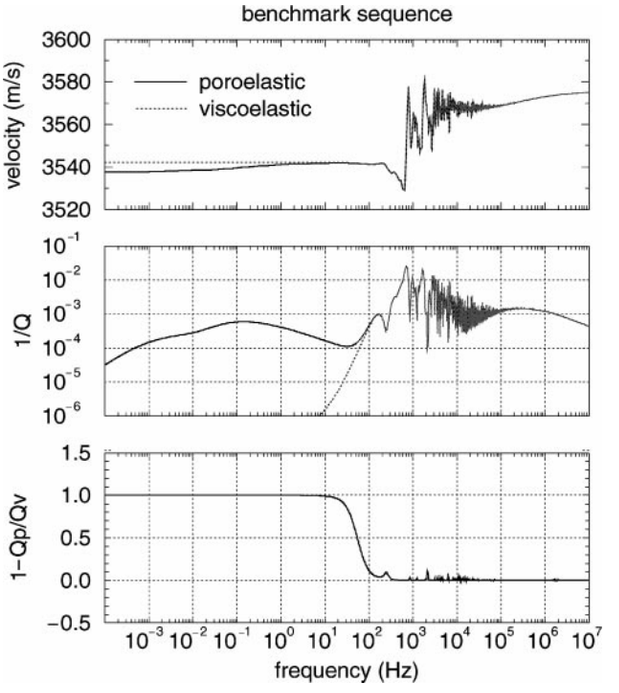

FIG. 6. Phase velocity, Q^{-1}, and the relative difference $(Q_p^{-1} - Q_v^{-1})/Q_p^{-1}$ for the benchmark synthetic sequence corresponding to the properties shown in Figure 5.

To do so, we increase the range of the frame-compliance factor to $12 < a < 24$, while keeping all other properties as in the benchmark sequence. The results are displayed in Figure 8. As expected, the location of the center frequency of the interlayer-flow attenuation is unaltered, but the level of this attenuation has been increased (Skempton's coefficient is larger). Slow-wave effects at higher frequencies are again more pronounced than in the benchmark example, which again is due to the fact that the amplitude of a generated slow-wave increases with rock compliance.

Dependence on the angle of incidence.—Next, we consider the effect of angle of incidence for the benchmark sequence. In the upper part of Figure 9, we show the fully poroelastic attenuation at four different angles of incidence. Except at the largest angle of 80° for which postcritical incidence holds at all interfaces in the stack, we see that the interlayer-flow attenuation is largely independent of the angle of the incidence. Interestingly, the high-frequency attenuation is strongly affected. In the lower part of the figure we compare the poroelastic attenuation at $\theta = 60°$ to the viscoelastic attenuation at $\theta = 0°$, 30° and 60°. We see that the high-frequency viscoelastic attenuation is roughly independent of angle of incidence. The large slow-wave effect being observed at high frequencies is due to the fact that the amplitude of generated slow-waves at isolated interfaces steadily increases with increasing angle of incidence.

A thin-layered sand sequence.—As a final example, we move away from the benchmark sequence and consider a stack having thinner, more compliant, and more permeable layers. Such a sequence might correspond to a shallow-sand sequence in a sedimentary basin with subtle layering effects being caused by variations in the sediment flux and grain sizes at time of burial. Stratification in many sandstones can be observed down to the centimeter scale or even smaller.

In this example we thus let the layers vary between 1 and 10 cm in thickness and let the lithological properties vary as $0.10 < \phi < 0.30, 20\,\mu\text{m} < \ell < 80\,\mu\text{m}, 10 < a < 24$. This range still corresponds to consolidated sediments. The sequence properties are shown in Figure 10, and the attenuation and dispersion are shown in Figure 11. An interesting effect in this example is that Q^{-1} is virtually constant across the surface-seismic band. Such a constant Q effect is entirely due to the interlayer flow, that is, Biot slow waves. It is somewhat robust with respect to different sequences of random numbers and also rather robust to variations in the permeability and compliance ranges. However, as should be expected from equation (2), it requires a wide range of layer thicknesses. If the range of layer thicknesses is restricted, for example, to just a few centimeters, the constant Q effect disappears. Finally, because the sands of this example are both compliant and permeable relative to, say, the well-consolidated Blackhawk formation, we find that there are significant slow-wave effects throughout the entire range of frequencies.

CONCLUSIONS

We have numerically modeled P-wave propagation in stratified sediments using Biot's (1962) theory. As understood and analytically modeled by previous authors, the equilibration of fluid pressure between adjacent layers in a stack can cause

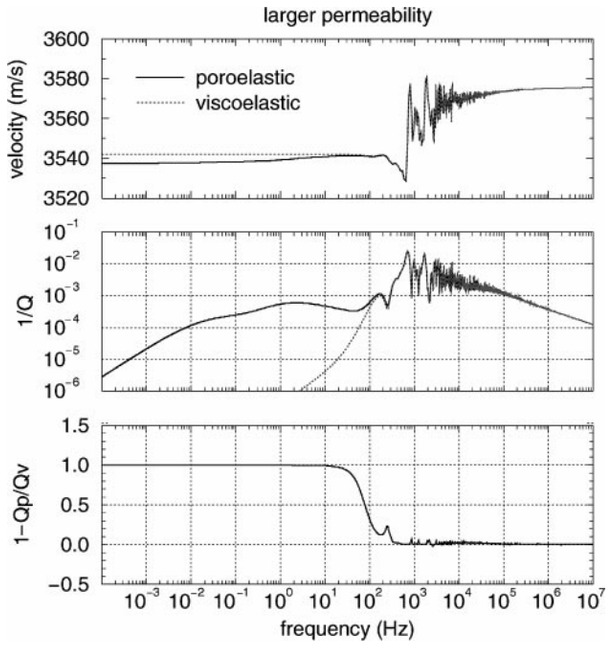

FIG. 7. Phase velocity, Q^{-1}, and the relative difference $(Q_p^{-1} - Q_v^{-1})/Q_p^{-1}$ for a high-permeability variant of the benchmark synthetic sequence. The mercury-breakthrough pore diameters ranged from 8 to 80 μm, corresponding to permeabilities roughly 16 times larger than that in Figure 5. The dominant effect is that the interlayer-flow attenuation peak is shifted to higher frequency.

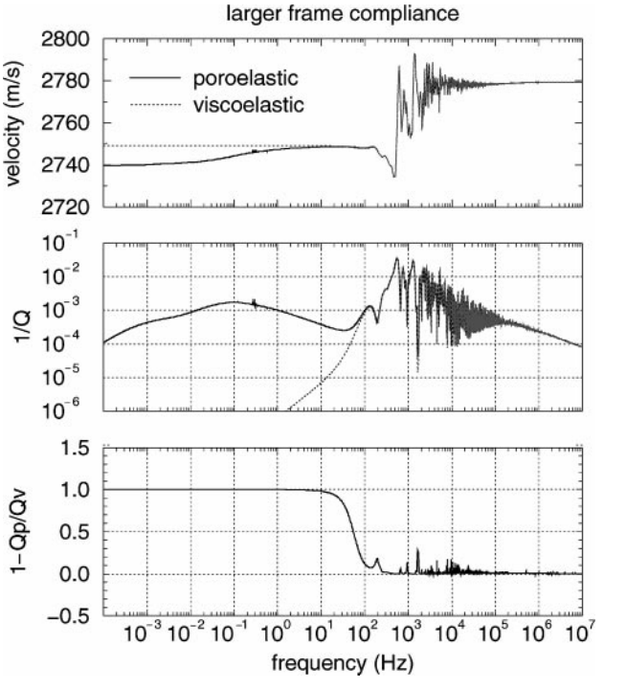

FIG. 8. Phase velocity, Q^{-1}, and the relative difference $(Q_p^{-1} - Q_v^{-1})/Q_p^{-1}$ for a larger-frame-compliance variant of the benchmark synthetic sequence. The compliance factors a of equation (17) are taken to lie in the range 12 to 24. The low-frequency attenuation has been increased in magnitude but unaltered in frequency relative to the benchmark.

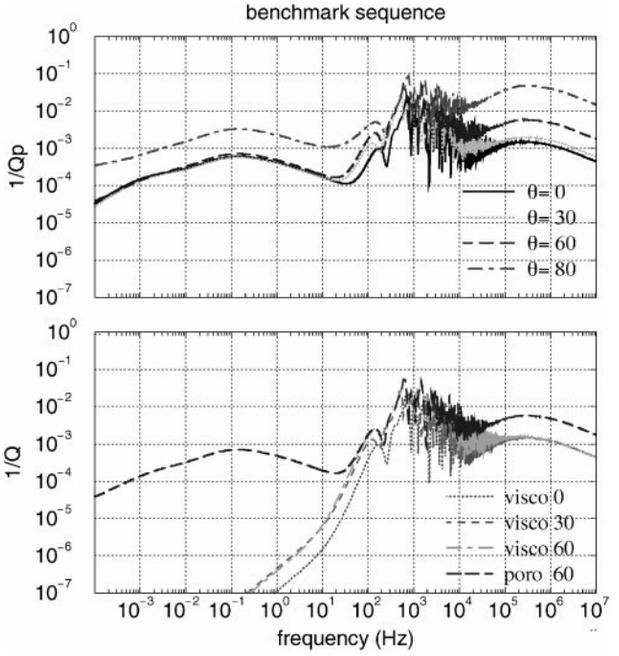

FIG. 9. The effect of angle of incidence on the transmitted amplitudes. The upper panel shows just the effects on the poroelastic attenuation; the lower panel shows the poroelastic attenuation at $\theta = 60^\circ$ compared to the viscoelastic attenuation at $\theta = 0^\circ$, 30°, and 60°. The interesting poroelastic effect is the increase of attenuation at very high frequencies due to the fact that slow waves are more easily generated at larger angles of incidence. The viscoelastic attenuation shows no such high-frequency increase with angle of incidence.

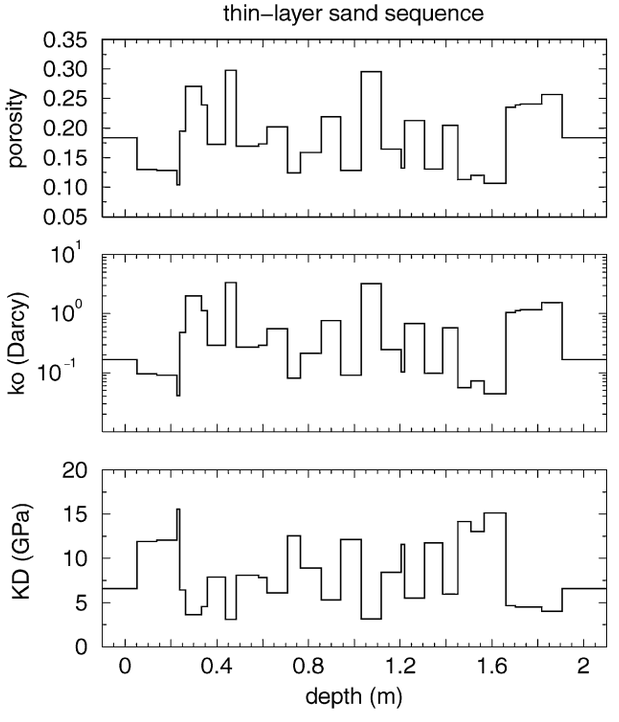

FIG. 10. The material properties corresponding to thin layers of sand having variable grain sizes. The layer thicknesses range from 1 to 10 cm.

significant attenuation in the surface-seismic band. Thinner layers and/or higher permeabilities shift the center frequency for these effects to higher frequencies as dictated by equation (2). In a typical sandstone formation, if the layer thicknesses are all taken to be greater than, say, 1 m, the interlayer-flow attenuation is pushed to frequencies below the surface-seismic band of interest. Sedimentary rocks have variations down to the centimeter scale, and it is likely that such slow-wave equilibration is the dominant source of low-frequency attenuation in a sedimentary basin. Because well logs usually only provide resolution of material properties down to the scale of about 1 m, they should not be used to generate the layer models for studying this effect. The slow-wave effects are enhanced in more compliant sediments due to the enhanced value of Skempton's coefficient. In a synthetic (but nonetheless reasonably realistic) sand sequence, virtually constant Q was observed across the entire surface-seismic band. Another new observation is that because slow-waves generated at an isolated interface have amplitudes that increase with both frequency and angles of incidence, they can significantly alter the predicted P-wave scattering. This can be up to a 50% effect in the normal-incidence examples considered here and as much as an order of magnitude at nonnormal incidence.

ACKNOWLEDGMENTS

S. R. P. would like to thank Serge Shapiro and Boris Gurevich for bringing their fine work on this problem to his attention. He would also like to thank the Geophysics Department at Stanford University and the Stanford Rock Physics and Borehole Consortium (SRB) for providing support during his sabbatical there. The work of J. G. B. was performed under the auspices of the U. S. Department of Energy by the University of California

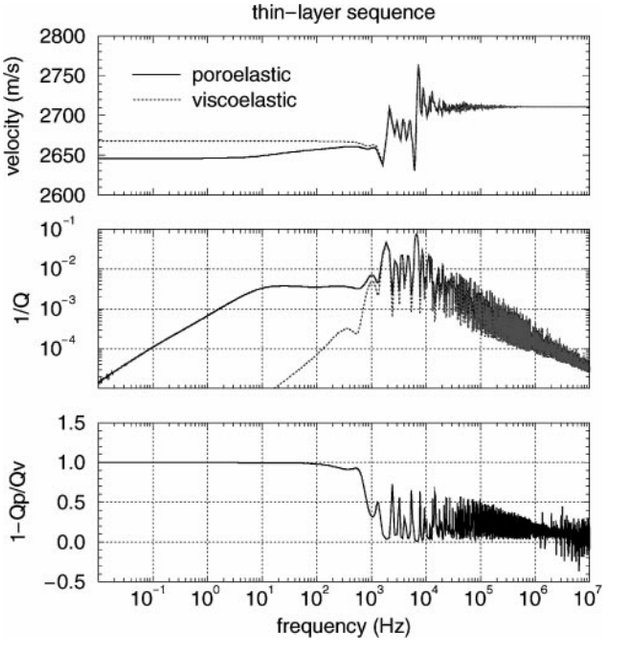

FIG. 11. Phase velocity, Q^{-1}, and the relative difference $(Q_p^{-1} - Q_v^{-1})/Q_p^{-1}$ for the thin layers of the sand model in Figure 10. The interesting feature here is the constant Q across the seismic band caused by the interlayer flow.

Lawrence Livermore National Laboratory under contract No. W-7405-ENG-48 and supported specifically by the Geosciences Research Program of the DOE Office of Energy Research within the Office of Basic Energy Sciences, Division of Engineering and Geosciences.

REFERENCES

Aki, K., and Richards, P. G., 1980, Quantitative seismology: W. H. Freeman & Co.

Berryman, J. G., 1980a, Long-wavelength propagation in composite elastic media I. Spherical inclusions: J. Acoust. Soc. Am. **68**, 1809–1819.

——— 1980b, Long-wavelength propagation in composite elastic media II. Ellipsoidal inclusions: J. Acoust. Soc. Am. **68**, 1820–1831.

Berryman, J. G., and Thigpen, L., 1985, Linear dynamic poroelasticity with microstructure for partially saturated porous solids: ASME J. Appl. Mech., **52**, 345–350.

Biot, M. A., 1956a, Theory of propagation of elastic waves in a fluid-saturated porous solid. I. Low-frequency range: J. Acoust. Soc. Am., **28**, 168–178.

——— 1956b, Theory of propagation of elastic waves in a fluid-saturated porous solid. II. Higher frequency range: J. Acoust. Soc. Am., **28**, 179–191.

——— 1962, Mechanics of deformation and acoustic propagation in porous media: J. Appl. Phys., **33**, 1482–1498.

Biot, M. A., and Willis, D. G., 1957, The elastic coefficients of the theory of consolidation: J. Appl. Mech., **24**, 594–601.

Chin, R. C. Y., Berryman, J. G., and Hedstrom, G. W., 1985, Generalized ray expansion for pulse propagation and attenuation in fluid-saturated porous media: Wave Motion, **7**, 43–66.

Deresiewicz, H., and Skalak, R., 1963, On uniqueness in dynamic poroelasticity: Bull. Seis. Soc. Am., **53**, 783–788.

Gelinsky, S., and Shapiro, S. A., 1997, Dynamic-equivalent medium approach for thinly layered saturated sediments: Geophys. J. Internat. **128**, F1–F4.

Gelinsky, S., Shapiro, S. A., Müller, T., and Gurevich, B., 1998, Dynamic poroelasticity of thinly layered structures: Internat. J. Solids Struct., **35**, 4739–4751.

Gurevich, B., and Lopatnikov, S. L., 1995, Velocity and attenuation of elastic waves in finely layered porous rocks: Geophys. J. Internat., **121**, 933–947.

Gurevich, B., and Schoenberg, M., 1999, Interface conditions for Biot's equations of poroelasticity: J. Acoust. Soc. Am., **105**, 2585–2589.

Hashin, Z., and Shtrikman, S., 1961, Note on a variational approach to the theory of composite elastic materials: J. Franklin Inst., **271**, 336–341.

Johnson, D. L., Koplik, J., and Dashen, R., 1987, Theory of dynamic permeability and tortuosity in fluid-saturated porous media: J. Fluid Mech., **176**, 379–402.

Kennett, B. L. N., 1983, Seismic wave propagation in stratified media: Cambridge Univ. Press.

Kennett, B. L. N., and Kerry, N. J., 1979, Seismic waves in a stratified half space: Geophys. J. Roy. Astr. Soc., **57**, 557–583.

Korringa, J., Brown, R. J. S., Thompson, D. D., and Runge, R. J., 1979, Self-consistent imbedding and the ellipsoidal model for porous rocks: J. Geophys. Res., **84**, 5591–5598.

Norris, A. N., 1993, Low-frequency dispersion and attenuation in partially saturated rocks: J. Acoust. Soc. Am., **94**, 359–370.

Plona, T. J., 1980, Observation of a second bulk compressional wave in a porous medium at ultrasonic frequencies: Appl. Phys. Lett., **36**, 259–261.

Pride, S. R., and Haartsen, M. W., 1996, Electroseismic wave properties: J. Acoust. Soc. Am. **100**, 1301–1315.

Shapiro, S. A., and Müller, T., 1999, Seismic signatures of permeability in heterogeneous porous media: Geophysics, **64**, 99–103.

Skempton, A. W., 1954, The pore-pressure coefficients A and B: Geotechnique, **4**, 143–147.

Thompson, A. H., Katz, A. J., and Krohn, C. E., 1987, The microgeometry and transport properties of sedimentary rock: Advances in Physics, **36**, 625–694.

White, J. E., Mikhaylova, N. G., and Lyakhovitsky, F. M., 1975, Low-frequency seismic waves in fluid-saturated layered rocks: Izvestija Academy of Sciences USSR, Phys. Solid Earth, **11**, 654–659.

APPENDIX A

THE REFLECTIVITY SCHEME

Kennett's reflectivity method (Kennett and Kerry, 1979) builds up the $\mathcal{R}_0$ and $\mathcal{T}_0$ matrices of equation (22) iteratively by starting at the top of the lower half-space and adding on one layer per iteration until the total-stack response is constructed. The recursion is obtained by simple intuitive reasoning and is exact. Imagine that we have a stack of layers in which the topmost interface is called ℓ and that we know the total-reflection matrix $\mathcal{R}_\ell$ and the total-transmission matrix $\mathcal{T}_\ell$ for this stack. Another layer is then added to the top of the stack so that the topmost interface is now $\ell-1$. If downward plane waves are incident on this topmost layer and if the reflection and transmission at interface $\ell-1$ as well as all internal reverberations within layer ℓ are included, one obtains the following recursion relations:

$$\mathcal{R}_{\ell-1} = R^d_{\ell-1} + T^u_{\ell-1}\bar{\mathcal{R}}_\ell\left(I - R^u_{\ell-1}\bar{\mathcal{R}}_\ell\right)^{-1}T^d_{\ell-1} \quad \text{(A-1)}$$

$$\mathcal{T}_{\ell-1} = \bar{\mathcal{T}}_\ell\left(I - R^u_{\ell-1}\bar{\mathcal{R}}_\ell\right)^{-1}T^d_{\ell-1} \quad \text{(A-2)}$$

$$\bar{\mathcal{R}}_\ell = E_\ell\mathcal{R}_\ell E_\ell \quad \text{(A-3)}$$

$$\bar{\mathcal{T}}_\ell = \mathcal{T}_\ell E_\ell. \quad \text{(A-4)}$$

The iteration begins with $\ell = L$, $\mathcal{R}_L = R^d_L$, and $\mathcal{T}_L = T^d_L$, and then counts backwards (adds layers) to $\ell = 1$. It uses the upward and downward reflection and transmission matrices $R^{u,d}_\ell$ and $T^{u,d}_\ell$ for each isolated interface ℓ as well as the phase-advancement diagonal matrix E_ℓ for each layer ℓ defined as

$$E_\ell = \text{diag}\{e^{i\omega q_P h_\ell}, e^{i\omega q_{\text{slow}} h_\ell}, e^{i\omega q_{SV} h_\ell}\}, \quad \text{(A-5)}$$

where the various q_ξ are the complex vertical slownesses for each wave type $\xi = P$, slow, SV. Although the index ℓ is suppressed, the q_ξ will be different in general for each layer. The vertical slownesses are related to the complex phase slownesses s_ξ and the real horizontal slowness p as

$$q^2_\xi + p^2 = s^2_\xi. \quad \text{(A-6)}$$

The q_ξ always have $\text{Im}\{q_\xi\} > 0$ and, as such, the elements of E_ℓ always have amplitudes less than one, so that the above recursion is numerically stable. The matrix I is the identity matrix, and the inverse matrix $(I - R^u_{\ell-1}\bar{\mathcal{R}}_\ell)^{-1}$ when expanded in series is seen to correspond to all the internal reverberations of the layer ℓ.

The reflection and transmission matrices at an isolated interface are determined from the boundary conditions that hold at a porous interface. Pride and Haartsen (1996) [c.f., Deresiewicz and Skalak (1963), Berryman and Thigpen (1985), and/or Gurevich and Schoenberg (1999)] have shown that for open and even partially sealed interfaces, the field components in the array

$$b = [u_x, u_z, w_z, \tau_{xz}, \tau_{zz}, -p]^T \quad \text{(A-7)}$$

must be continuous. Thus, the boundary condition at interface ℓ is simply

$$b_\ell = b_{\ell+1}. \quad \text{(A-8)}$$

Deresiewicz and Skalak (1963) introduced the notion of an interface permeability which can be given some justification

when there exists a thin layer of transition material separating two porous materials and when it is desired to allow for such a thin layer implicitly using an "effective" boundary condition. But in this case, all the components (not just the fluid pressure) can suffer jumps at the interface, and this fact was not properly considered by Deresiewicz and Skalak. In the present work, such thin layers are modeled explicitly so that no such effective boundary conditions are required.

The response b at a given point in a given layer is the sum of all the various upgoing and downgoing plane waves that are present at that point. Following Kennett and Kerry (1979), the first-order array w is defined to contain the various plane-wave amplitudes

$$w = [\mathrm{u_P}, \mathrm{u_{slow}}, \mathrm{u_{SV}}, \mathrm{d_P}, \mathrm{d_{slow}}, \mathrm{d_{SV}}]^T, \tag{A-9}$$

and can be written in the partitioned form $w = [\mathrm{u}, \mathrm{d}]^T$. Similarly, the matrix D is defined to have columns that contain the normalized response of each of the six types of plane waves in a uniform material

$$D = \left[b^u_{\mathrm{P}}, b^u_{\mathrm{slow}}, b^u_{\mathrm{SV}}, b^d_{\mathrm{P}}, b^d_{\mathrm{slow}}, b^d_{\mathrm{SV}}\right], \tag{A-10}$$

where each $b^{u,d}_\xi$ vector has the physical components defined by equation (A-7). Thus, the total material response b at a given point is simply

$$b = Dw. \tag{A-11}$$

The columns of D are often called the eigenvectors of the governing equations (3)–(6), while the ωq_ξ are the eigenvalues. Pride and Haartsen (1996) determined such plane-wave response exactly for porous media, and we simply state their results here.

For the longitudinal-wave response $b^{u,d}_\xi$ with $\xi = P$, slow, we have

$$b^{u,d}_\xi = \begin{bmatrix} p/s_\xi \\ \pm q_\xi/s_\xi \\ \pm q_\xi \beta_\xi/s_\xi \\ \pm 2i\omega G p q_\xi/s_\xi \\ i\omega s_\xi \left(H - 2Gp^2/s^2_\xi + \beta_\xi C\right) \\ i\omega s_\xi (C + M\beta_\xi) \end{bmatrix}, \tag{A-12}$$

where β_ξ is an auxiliary term defined as

$$\beta_\xi = -\frac{Hs^2_\xi - \rho}{Cs^2_\xi - \rho_f}. \tag{A-13}$$

The two longitudinal-wave phase slownesses are given by

$$2s^2_{\mathrm{P,slow}} = \gamma \mp \sqrt{\gamma^2 - 4\frac{\rho\tilde{\rho} - \rho^2_f}{MH - C^2}}, \tag{A-14}$$

where γ is another auxiliary term

$$\gamma = \frac{\rho M + \tilde{\rho} H - 2\rho_f C}{MH - C^2}, \tag{A-15}$$

and where

$$\tilde{\rho} = \frac{i}{\omega}\frac{\eta}{k(\omega)} \tag{A-16}$$

defines the effective inertia of the fluid in relative motion. The transverse-wave response $b^{u,d}_{\mathrm{SV}}$ is

$$b^{u,d}_{\mathrm{SV}} = \begin{bmatrix} \pm q_{\mathrm{SV}}/s_{\mathrm{SV}} \\ -p/s_{\mathrm{SV}} \\ -(\rho_f/\tilde{\rho})p/s_{\mathrm{SV}} \\ i\omega G\left(q^2_{\mathrm{SV}} - p^2\right)/s_{\mathrm{SV}} \\ \mp 2i\omega G q_{\mathrm{SV}} p/s_{\mathrm{SV}} \\ 0 \end{bmatrix}, \tag{A-17}$$

where the transverse-wave phase slowness is

$$s^2_{\mathrm{SV}} = \frac{\rho - \rho^2_f/\tilde{\rho}}{G}. \tag{A-18}$$

All of these plane-wave responses have been normalized with respect to the solid displacements.

Finally, to obtain the required isolated-interface reflection and transmission matrices, we use the notation of Kennett and Kerry (1979) and write the eigenvector matrix in the partitioned form

$$D_\ell = \begin{bmatrix} M^u_\ell & M^d_\ell \\ N^u_\ell & N^d_\ell \end{bmatrix}, \tag{A-19}$$

where the M partitions correspond to the displacements and the N partitions to the stresses. The downward reflection/transmission matrices are obtained by imposing downward waves incident from above on an isolated interface ℓ. We thus write the plane-wave amplitudes just above the interface in the partitioned form $w_\ell = [\mathrm{u}, 1]^T$ and the amplitudes just below the interface as $w_{\ell+1} = [0, \mathrm{d}]^T$, so that the downward reflection/transmission matrices are defined by $\mathrm{u} = R^d_\ell \cdot 1$ and $\mathrm{d} = T^d_\ell \cdot 1$. The upward reflection/transmission matrices are similarly defined by imposing upward waves incident from below at the same interface. Using the continuity condition $b_\ell = b_{\ell+1}$ and the representation $b = Dw$ then gives

$$R^d_\ell = -\left[N^u_\ell - N^d_{\ell+1}\left(M^d_{\ell+1}\right)^{-1} M^u_\ell\right]^{-1} \times \left[N^d_\ell - N^d_{\ell+1}\left(M^d_{\ell+1}\right)^{-1} M^d_\ell\right], \tag{A-20}$$

$$T^d_\ell = \left(M^d_{\ell+1}\right)^{-1}\left[M^d_\ell + M^u_\ell R^d_\ell\right], \tag{A-21}$$

$$R^u_\ell = -\left[N^d_{\ell+1} - N^u_\ell\left(M^u_\ell\right)^{-1} M^d_{\ell+1}\right]^{-1} \times \left[N^u_{\ell+1} - N^u_\ell\left(M^u_\ell\right)^{-1} M^u_{\ell+1}\right], \tag{A-22}$$

$$T^u_\ell = \left(M^u_\ell\right)^{-1}\left[M^u_{\ell+1} + M^d_{\ell+1} R^u_\ell\right]. \tag{A-23}$$

All formulas have now been given that are used to determine the reflection from and transmission through a stack of porous layers as a function of (ω, p).